Trident Research Campaigns

D. S. Montgomery, R. P. Johnson, J. A. Cobble, J. C. Fernandez, A. A. Hauer, and G. A. Kyrala (P-24); E. L. Lindman (XTA); H. A. Rose (T-13); and K. G. Estabrook (Lawrence Livermore National Laboratory)

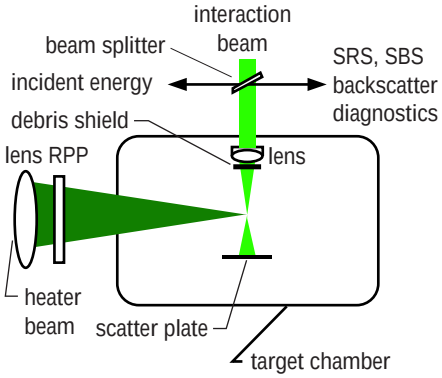

Fig. 1 Schematic top-view of the laser beam and diagnostic configurations used in the single hot-spot interaction experiments.

Introduction

During the past two years, the Trident laser facility has provided over 2,200 laser shots for 25 different experimental campaigns involving experimentalists from Los Alamos National Laboratory, Sandia National Laboratory, Lawrence Livermore National Laboratory, and colleges and universities around the country and the world, including Imperial College and Oxford University in the United Kingdom, Ecole Polytechnique in France, the University of Maryland, the University of Michigan, and the University of California at San Diego. Roughly one-quarter of the Trident experimental campaigns have been fielded by personnel from the Los Alamos Plasma Physics Group (P-24) for diagnostic development or testing of diagnostics in preparation for experiments at Trident or Livermore's Nova or the University of Rochester's Omega laser systems. The remaining experimental campaigns have been independent experimental campaigns fielded to address the individual goals of various universities or to support the goals of the local Inertial Confinement Fusion (ICF) Program. Most of the laser time was devoted to two major experimental programs, one to study laser plasma instabilities and the other to study dynamic properties of materials. University users were also involved as collaborators in these two very important areas.

Most campaigns were carried out on the main Trident target chamber, but a number of campaigns were accomplished on two auxiliary target chambers using Trident's short-pulse capability. Some of these involved diagnostic development, testing, and calibration while others addressed the nature of the interaction of a very high-intensity laser pulse with a plasma. These latter campaigns were conducted to test aspects of the fast-ignitor concept for ICF ignition at the National Ignition Facility (NIF).

This research highlight will focus on the two experimental campaigns that used most of the laser time. The first is sponsored by the Laboratory Directed Research and Development (LDRD) Program to study laser plasma instabilities. Its focus is to study the interaction of a single laser hot spot with a pre-formed plasma with a view to understanding, in more realistic laser beams, the parametric scattering instabilities that pose a threat to ICF ignition. The second campaign, part of the dynamic properties of materials program, focussed on developing experimental techniques to study shock-induced melt and other phase transformations in materials under the extreme conditions of interest to ICF and weapons physics. These campaigns are discussed individually below.

Characterizing Plasma and Laser Conditions for Single Hot-Spot Interaction Experiments

Laser beams are scattered by density fluctuations (waves) in a plasma because these fluctuations alter the index of refraction that the laser encounters. With low amplitude waves, this process (called collective Thomson scattering) is benign, and it provides a powerful tool for diagnosing plasma conditions. On the other hand, stimulated scattering involves the unstable growth of waves in the

plasma fed by the laser energy. These waves can scatter a significant fraction of the laser energy in undesirable directions. Stimulated scattering by electron plasma waves (Raman scattering) and ion-acoustic waves (Brillouin scattering) poses a significant threat to ICF.

The Trident laser system was used for fundamental experiments addressing the interaction of laser self-focusing, stimulated Raman scattering (SRS), and stimulated Brillouin scattering (SBS) in a near-diffraction-limited (single) laser hot spot under ICF-relevant plasma conditions. Our aim was to gain a better understanding of the coupling between these plasma instabilities. This laser-plasma system is sufficiently small for direct modeling by an emerging suite of computer codes incorporating new theoretical models. If we succeed in understanding this system, we hope to develop simpler models suitable for quantitative predictions in much larger ignition plasmas. The first step in this process is to create an ignition-relevant plasma and to characterize it thoroughly and accurately.

In our investigation, one of Trident's three 527-nm laser beams was used to create and heat a long-scale-length plasma (~1 mm, ~0.6 keV). A second, lower-energy Trident beam was then used to produce a nearly diffraction-limited interaction laser beam with minimal wave-front distortion incident in the target plasma. Figure 1 shows a schematic of the laser and diagnostic configuration used in our experiments.

The plasma heater beam was focused with an $f/6$ aspheric lens and a "stripline" random phase plate (RPP), which produces a line focus with dimensions of ~100-μm high × 1,000-μm long.[1] The laser energy is 160 ± 10 J in a 1.3-ns pulse at constant power with 100-ps rise and fall times. It illuminates a 1-mm-diameter plastic or aluminum target at normal (perpendicular) incidence with the line focus in the horizontal plane. The interaction beam was focussed on the target using an air-spaced achromat lens with a 250-mm focal length (f) positioned at $f/7$. This lens was mounted inside the vacuum chamber where the plasma is generated, so a high-quality debris shield was placed between the lens and target to protect the lens. The interaction beam was incident 90° to the heater beam and was offset parallel to the target surface by between 100 and 400 μm to vary the sampled plasma density. The 200-ps interaction beam was delayed by 1.8 ± 0.05 ns with respect to the beginning of the heater beam so that the heater beam was off when the interaction pulse was on. This delay is important because it removes any influence of the heater beam on the experiment.

A beam splitter was placed in the interaction beam to sample the incident beam energy and the reflected light from the plasma scattering processes. The extensive diagnostics for the scattered light on Trident, used to study SRS and SBS, are beyond the scope of this article and will not be described.

To characterize the interaction laser, we measured the focal plane intensity distribution using a 40× microscope objective and a charge-coupled device (CCD) camera. Figure 2 shows an image of the interaction laser at best focus (a) and an azimuthally averaged

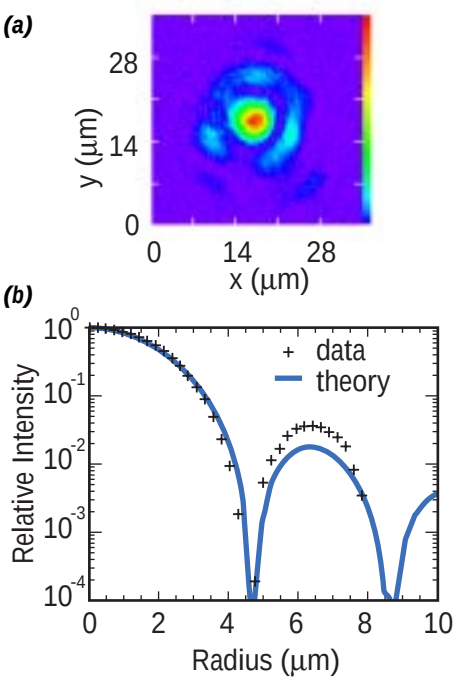

Fig. 2 (a) Far-field image of the single hot spot beam (the colors represent light intensity with red being the highest, blue being the lowest, and black being no intensity). (b) Azimuthally averaged radial profile of the far field data, with diffraction from an ideal f/7 beam superimposed.

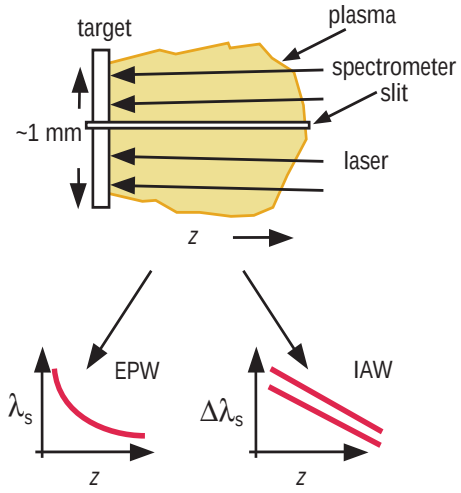

***Fig. 3** Schematic bottom-view of the target and the imaging spectrometer orientation with respect to the target and heater beam for Thomson scattering measurements. The graphs show a cartoon of the expected scattering from EPWs and IAWs for this configuration.*

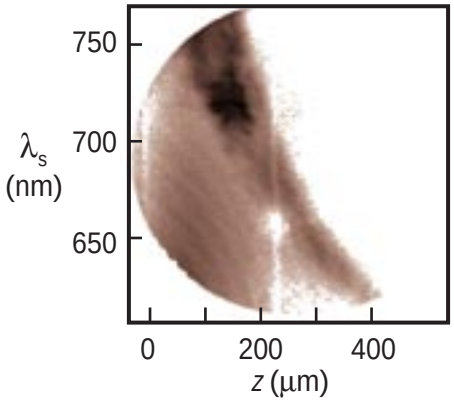

***Fig. 4** Scattering from EPWs as a function of distance from the target surface at t = 1.0 ± 0.1 ns for a plastic plasma. The vertical features at z = 0 and z = 200 μm are artifacts due to dead spots on the detector.*

radial profile (b). Superposed is the theoretical radial profile for diffraction from a plane wave incident on a circular aperture at *f*/7 (the theoretical ideal performance), which is in excellent agreement with the measured results.

The interaction laser beam has a full-width at half maximum (FWHM) of 3.8 ± 0.15 μm, and it produces a peak intensity of 1×10^{16} W/cm^2 for a nominal energy of 0.8 J (maximum) in a 200-ps FWHM Gaussian pulse. The peak intensity can be adjusted between 10^{14} and 10^{16} W/cm^2 using polished, calibrated neutral density filters.

We measured the angular distribution of the transmitted interaction laser by having the transmitted beam illuminate a diffuser, which was then imaged onto a CCD camera filtered for 527 ± 5 nm. The camera system was absolutely calibrated so that transmitted energy measurements were obtained. This measurement, which is important to diagnose the laser-plasma instabilities, will not be discussed further.

To characterize the plasma, we used a 5-cm focal length, *f*/6 achromat to collect Thomson scattered light at 90° from the heater beam. The target was imaged onto the slit of a 0.5-m imaging spectrometer with the image oriented along the direction of the plasma expansion, perpendicular to the target surface. The output of the spectrometer was coupled to a gated optical camera with ~120-ps frame time and the image was recorded using a CCD camera. The spectrometer was operated in either low or high dispersion to measure Thomson-scattered signals from electron plasma waves (EPWs) or ion acoustic waves (IAWs).

A schematic of the Thomson scattering measurement is given in Fig. 3, which also shows the slit orientation with respect to the target image. The sampled scattering volume at the target plane was ~10 μm wide (slit width) with ~100-μm line-of-sight depth through the plasma. The imaging direction of the spectrometer is oriented along the plasma-expansion direction, allowing reconstruction of the scattered-light profile with a 25-μm resolution.

Scattering from EPWs was examined to obtain measurements of the plasma density profile. Using the dispersion relations for the EPWs and scattered light, the scattered light should go from long wavelength near the target surface to shorter wavelength farther away as the density goes from high to low, as indicated in the graph in Fig. 3. Figure 4 shows a corresponding measurement of scattering from EPWs versus distance from the target near the end of the heater pulse (t = 1.0 ± 0.1 ns) for a 6.5-μm-thick plastic target. The spectrum at a given distance from the target surface shows a cutoff at a maximum wavelength, which corresponds to the peak density at that position. A density profile is obtained from the data by finding the edge of the maximum wavelength cutoff versus position, and assuming an electron temperature, T_e, equal to 0.5 ± 0.1 keV in the dispersion relations. A plot of the inferred electron density, n_e/n_{cr}, where n_{cr} is the critical density ($n_{cr} = 4 \times 10^{21}$ cm^{-3}, above which 527-nm light does not propagate), *vs.* position from the target surface is shown in Fig. 5.

Collective Thomson scattering from IAWs is used to measure profiles of electron temperature (T_e), ion temperature (T_i), and flow velocity (v_z). The scattering geometry determines the wave-number of the IAWs being probed and is given by $k_{IAW} = 2k_0 \sin(\Theta/2)$, where $k_0 = 2\pi/\lambda_0$ is the laser wave-number, and Θ is the angle between the incident and scattered light. The dispersion relations indicate that the separation between the upshifted and downshifted IAWs is a function of T_e, and the flow velocity produces a Doppler shift of the entire spectrum, as indicated in the graph in Fig. 3 for an isothermal plasma, which turns out to be a good assumption. A corresponding measurement of Thomson-scattered light from IAWs *vs.* distance is shown in Fig. 6 near the end of the heater pulse ($t = 1.0 \pm 0.1$ ns) for a 6.5-μm thick plastic target. The separation between the upshifted and downshifted waves is clearly resolved, and the entire spectrum becomes more Doppler shifted further from the target surface, indicating an increased flow speed at increased separation from the target surface.

A spectral lineout taken at the location $z = 300 \pm 25$ μm is shown in Fig. 7. The spectrum is asymmetric, indicating a relative drift between electrons and ions, and is due either to transport effects or

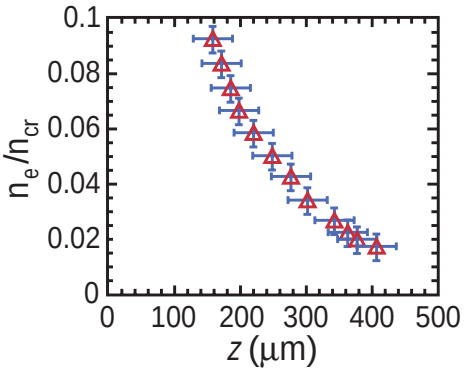

***Fig. 5** The electron density profile* **vs.** *distance from the target surface obtained from the EPW data shown in Fig. 4.*

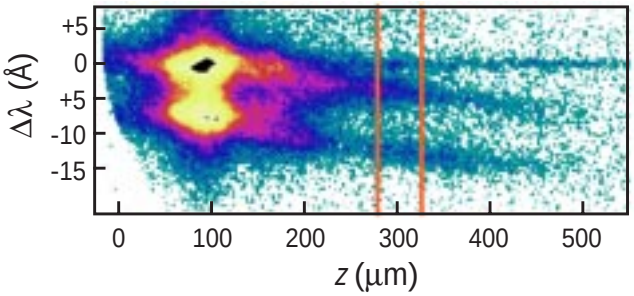

***Fig. 6** Scattering from IAWs as a function of distance from the target surface at* **t = *1.0 ± 0.1* ns for a plastic plasma.**

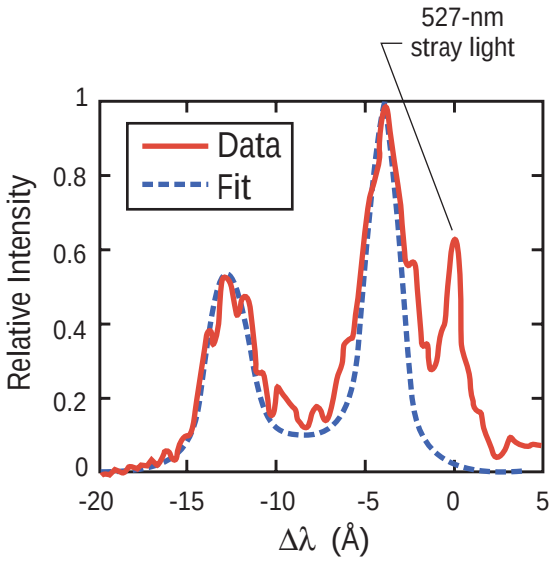

***Fig. 7** Spectral profile taken from the IAW data shown in Fig. 6 at* **z = *300 ± 25* μm.** *Superimposed is a fit for the Thomson scattering form factor for a fully ionized plastic plasma, with fit parameters* **T_e = *0.7 ± 0.1* keV, T_i = *0.14 ± 0.05* keV,** *and* **v_z = *4.8 ± 0.4* x 10^7 cm/s.** *The spectral line at $\Delta\lambda$ = 0 is due to stray 527-nm light, which provides a convenient wavelength fiducial.*

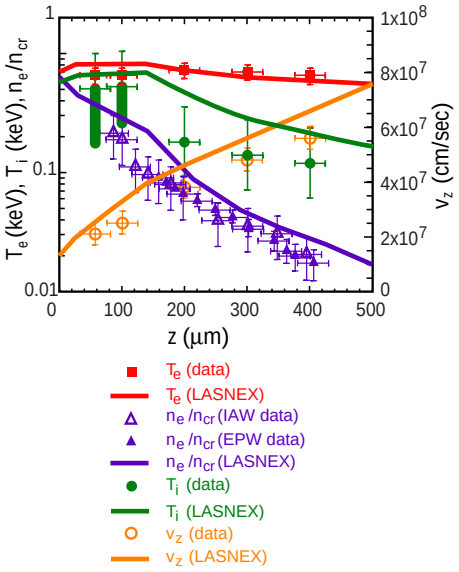

Fig. 8 Plot of electron density (n_e/n_{cr}), electron temperature (T_e), ion temperature (T_i), and flow velocity (v_z) profiles at $t = 1.0 \pm 0.1$ ns measured by Thomson scattering from the EPW and IAW data shown in Figs. 4 and 6. Simulated plasma profiles from 2-D LASNEX calculations are also shown.

to stimulated processes. The separation between peaks is mostly dependent on electron temperature, T_e, and weakly dependent on ion temperature, T_i. The width of each peak and the contrast between the center of the spectrum and the peak heights are dependent on T_i, and the overall Doppler shift from λ_0 depends on flow velocity. The entire spectrum is fitted using the Thomson scattering form factor for multi-ion species plasmas[2], and is used to determine T_e, T_i at that position. The flow velocity, v_z, is determined assuming that the dominant flow component is mostly parallel to the heater beam. Figure 8 shows the experimentally measured profiles of n_e/n_{cr}, T_e, T_i, and v_z at $t = 1.0 \pm 0.1$ ns for a plastic target derived from the Thomson scatter data shown in Figs. 4 and 6. Calculations of the plasma profiles using the 2-D hydrodynamics code LASNEX[3] are also shown as lines in Fig. 8 and are in rough agreement with the measurements. These data can be used to further refine the simulations for the experimental design.

In summary, we have produced ignition-relevant long-scale plasmas on Trident. The plasma conditions have been characterized with unprecedented detail using Thomson scattering. A nearly diffraction-limited laser beam suitable for interaction experiments has been produced and thoroughly characterized. Given these measurements, theoretical simulations of laser-plasma instability processes will be performed, and detailed comparisons to measurements will be made. We expect to gain sufficient understanding of these processes to allow the development of models suitable for quantitative predictions on ignition-scale plasmas.

Shock Wave Physics and High Pressure Materials Science Research

P-24, in collaboration with Los Alamos National Laboratory's Materials Science and Technology (MST), Dynamic Experimentation (DX), Applied Theoretical and Computational Physics (X), and Theoretical (T) Divisions, as well as Oxford University, Livermore, Sandia, the University of California at San Diego, and the University of Edinburgh, pursues an active research program in shock-wave physics and related materials science. The Trident laser system is used to drive moderate to high-pressure shock waves into condensed-state materials, and the response of the materials is diagnosed with an array of advanced diagnostics. These measurements are used to determine dynamic properties of materials that are of importance to the inertial fusion and the weapons programs. A modest-size laser system like Trident is well suited to certain areas of high-pressure materials science, providing accurate and flexible control over the temporal profile of shock generation, a wide range of achievable pressures (~0.05–30 Mbar), and very bright x-ray sources accurately synchronized to the shock generation. In addition, many shots can be fielded rapidly for accurate studies of various parameters. This section gives a brief review of some of the recent high-pressure materials work on the Trident laser.

A typical configuration for Trident materials science experiments is shown in Fig. 9. In this particular case the principal diagnostic method was transient x-ray diffraction[4], a method to which Trident experiments have made significant contributions. One beam of the laser system is used to drive a shock wave into the sample. Another beam is used to generate an intense x-ray source, in this case a point source of 6.1-keV radiation. In this example the x-rays diffract off planes roughly parallel to the entrance surface. This mode of diffraction is referred to as Bragg diffraction. As the shock wave reaches the rear surface of the crystal, the lattice planes are compressed and the Bragg angle of diffraction is changed. The angular deflection of the diffracted x-ray beam is thus directly proportional (through Bragg's law) to the real time-strain induced in the crystal by the shock wave. An example of typical data obtained using such a configuration is given in Fig. 10.

The x-ray streak record shown in Fig. 10 illustrates several important aspects of the shock propagation and its effect on the diffraction of x-rays. The lower portion of the streak represents diffraction from unshocked material before the shock wave has reached the rear surface of the crystal. As the shock comes within the probe distance of the x-rays, a portion of the diffracted x-rays are deflected to a higher angle and thus strike the streak camera slit at a different position. The separation of this streak from the uncompressed portion is directly proportional through Bragg's law to the strain induced in the crystal by the shock wave. The strains induced are typically large, on the order of a few percent. The strain rates are also quite large, ranging from 10^7 to 10^9 s^{-1}. The dynamics of solid-solid phase changes is one important phenomenon that can be studied by such methods.

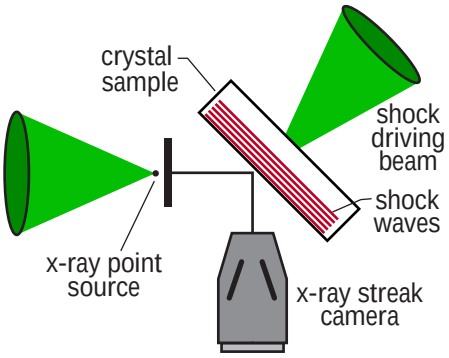

Fig. 9 A typical experimental configuration used on the Trident laser for shock wave and materials science studies.

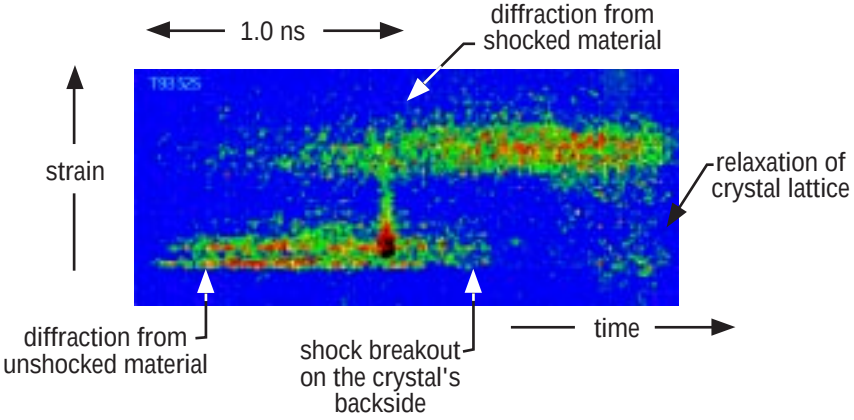

Fig. 10 Typical example of transient diffraction data obtained in shock wave materials research on the Trident laser. The peak shock pressure was about 150 kbar.

Figure 11 illustrates typical data from phase change studies. The several shots displayed represent a progression of increasingly higher shock pressure (generated by higher laser irradiances). In this case the diffraction is occurring from the <400> planes of a silicon crystal. At a particular threshold in pressure, the crystal goes through a phase change from the normal diamond cubic configuration to another configuration, most likely a body-centered tetragonal configuration. In the highest-pressure streak, the diffraction from compressed material is seen to split into two components indicative of the phase change. Through records of this sort, the dynamic properties of the phase change can be studied. These data are currently being compared with hydrodynamic simulations that include a new multiphase equation of state. This equation of state takes into account the observed phase change. Recent simulations using this multiphase equation of state have predicted that the dynamic threshold for this phase change should occur at about 200 kbar, which is quite close to the threshold that is observed experimentally. The next stage of this research will extend this work to another phase change: melt.

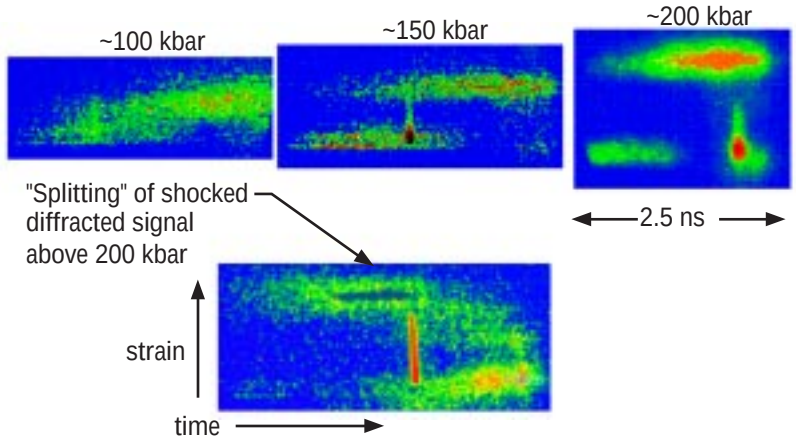

Fig. 11 Transient diffraction data from a material undergoing a shock-induced phase change.

Other materials science work on Trident focuses on plastic wave generation. Plastic behavior of materials occurs when shock waves have pressures above the elastic limit. Typically, condensed matter subjected to pressures above the elastic limit yields through generation of dislocations and other faults in the crystalline structure. One method for diagnosis and analysis of these fault generation mechanisms is post-shot analysis of the materials. Special systems “catch” the fragments of material after the shock event. Thin slices of the material are then subjected to analyses such as transmission electron microscopy. An example of this analysis is given in Fig. 12. The characteristic dislocation signatures indicate where the material has yielded when subjected to the high-pressure shock wave. The next stage of this research will compare the dislocation generation with molecular dynamics modeling. Molecular dynamics modeling is the most basic, first-principles approach to predicting the response of condensed materials to high-pressure shock waves. (The comparisons will be made with molecular dynamics calculations performed by Brad Holian and his

colleagues in T-11 and T-12.) It represents a first step in building a comprehensive picture of material behavior beginning at the atomic level and progressing to dislocation generation and finally macroscopic faults. The data obtained in experiments such as these can help to critique and benchmark this modeling.

Experiments on the Trident laser system have provided useful data on the dynamic properties of materials. In particular, we have developed new transient x-ray diffraction methods for studying the temporal structure of shock-induced solid phase changes, and methods for post-shot analysis of shock-induced dislocation generation. In addition, experimental data on phase changes have been compared with hydrodynamic modeling that uses the most advanced multiphase equations of state. The thresholds for the phase change predicted by the modeling agree well with experimentally observed values.

Trident experiments have also provided a useful test bed for developing new measurement methods and techniques that can be applied to larger-scale materials work on pulsed-power machines, gas guns, and explosive facilities. This review represents only a short summary of the broad range of materials research that we conduct using high-power radiation sources and pulsed-power radiation generators. We believe that this research will provide a useful supplement to traditional methods relying on explosives to generate the high pressures.

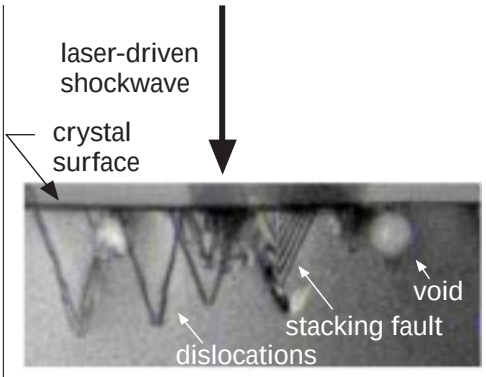

Fig. 12 Electron microscopy analysis of dislocations generated by a high-pressure laser-driven shock wave.

References

[1]B. S. Bauer, R. P. Drake, K. G. Estabrook, J. F. Camacho, R. G. Watt, M. D. Wilke, G. E. Busch, S. E. Caldwell, and S. A. Baker, “Meeting the Challenge of Detecting Ion-Plasma Waves,” *Physics of Plasmas* 2, 2207 (1995).

[2]D. E. Evans, "The Effect of Impurities on the Spectrum of Laser Light Scattered by a Plasma," *Plasma Physics* 12, 537 (1970).

[3]G. Zimmerman and W. Kruer, "Numberical Simulation of Laser-Initiated Fusion," *Comments on Plasma Physics and Controlled Fusion* 2, 51 (1975).

[4] A. A. Hauer and G. A. Kyrala, “Laser-Plasma X-Ray Emission: Its Creation, Diagnosis and Application in Transient Diffraction,” in *Time Resolved Diffraction*, J. R. Helliwell and P. M. Rentzepis, Eds. (Oxford Clarendon Press, Oxford, 1997), pp. 71–103.